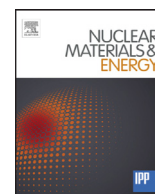


Contents lists available at ScienceDirect

Nuclear Materials and Energy

journal homepage: www.elsevier.com/locate/nme

Simulation of W dust transport in the KSTAR tokamak, comparison with fast camera data

A. Autricque^{a,*}, S.H. Hong^b, N. Fedorczak^a, S.H. Son^b, H.Y. Lee^{c,d}, I. Song^{c,d}, W. Choe^{c,d},
C. Grisolia^a

^aCEA, IRFM, Saint-Paul-Lez-Durance, F-13108, France

^bNational Fusion Research Institute, 113 Gwahangno, YuSung-Gu, Daejeon 305-333, Republic of Korea

^cDepartment of Physics, Korea Advanced Institute of Science and Technology (KAIST), Daejeon 34141, Republic of Korea

^dImpurity and Edge plasma Research Center, KAIST, Daejeon 34141, Republic of Korea

ARTICLE INFO

Article history:

Received 13 July 2016

Revised 8 November 2016

Accepted 9 November 2016

Available online xxx

ABSTRACT

In this paper, dust transport in tokamak plasmas is studied through both experimental and modeling aspects. Image processing routines allowing dust tracking on CCD camera videos are presented. The DUMPRO (DUSt Movie PROcessing) code features a dust detection method and a trajectory reconstruction algorithm. In addition, a dust transport code named DUMBO (DUSt Migration in a plasma BOundary) is briefly described. It has been developed at CEA in order to simulate dust grains transport in tokamaks and to evaluate the contribution of dust to the impurity inventory of the plasma. Like other dust transport codes, DUMBO integrates the Orbital Motion Limited (OML) approach for dust/plasma interactions modeling. OML gives direct expressions for plasma ions and electrons currents, forces and heat fluxes on a dust grain. The equation of motion is solved, giving access to the dust trajectory. An attempt of model validation is made through comparison of simulated and measured trajectories on the 2015 KSTAR dust injection experiment, where W dust grains were successfully injected in the plasma using a gun-type injector. The trajectories of the injected particles, estimated using the DUMPRO routines applied on videos from the fast CCD camera in KSTAR, show two distinct general dust behaviors, due to different dust sizes. Simulations were made with DUMBO to match the measurements. Plasma parameters were estimated using different diagnostics during the dust injection experiment plasma discharge. The experimental trajectories show longer lifetimes than the simulated ones. This can be due to the substitution of a boiling/sublimation point to the usual vaporization/sublimation cooling, OML limitations (eventual potential barriers in the vicinity of a dust grain are neglected) and/or to the lack of a vapor shielding model in DUMBO.

© 2016 The Authors. Published by Elsevier Ltd.

This is an open access article under the CC BY license (<http://creativecommons.org/licenses/by/4.0/>).

1. Introduction

Dust will be a critical issue for future fusion devices such as ITER. Generated through various processes related to plasma/wall interactions, dust grains are an important source of impurities having well known consequences in terms of radiative losses and plasma instabilities generation [1]. Dust can be observed using CCD cameras as they interact with the plasma, through recycling photon emission and thermal emissivity. Cameras provide with videos on which image processing routines can be applied in order to detect dust events and measure dust trajectories.

In [Section 2](#), the DUMPRO (DUSt Movie PROcessing) routines developed at CEA to extract dust trajectories is presented. In the case of intrinsic dust, the experimental data obtained by image processing is delicate to analyze, since a dust trajectory depends on the dust material, temperature, size and electric charge, among others. Dust injection was performed in several tokamaks and allows constriction of some of these parameters. Several codes dedicated to the modeling of dust transport in plasmas already exist, namely MIGRAINE [2], DUSTT [3] and DTOKS [4], among others.

In [Section 3](#), the newly developed DUMBO (DUSt Migration in a plasma BOundary) code will be briefly presented. The aim of this work is to prepare for the installation of a dust gun-type injector on the WEST tokamak, as well as the image processing and simulation tools developed for data analysis. Since the injector design is similar to that of the KSTAR dust injector [5], the 2015 KSTAR

* Corresponding author.

E-mail address: adrien.autricque@cea.fr (A. Autricque).

<http://dx.doi.org/10.1016/j.nme.2016.11.012>

2352-1791/© 2016 The Authors. Published by Elsevier Ltd. This is an open access article under the CC BY license (<http://creativecommons.org/licenses/by/4.0/>).

dust injection experiment will be analyzed using these tools, as an example, in Section 4.

2. DUMPRO: the image processing code

In tokamak operation, the commonly used diagnostic to obtain measurements on in-vessel dust transport is CCD cameras. They provide with RGB (Red-Green-Blue) videos that need further processing for dust events to be detected. In this section are detailed the DUMPRO (DUSt Movie PROcessing) routines used to detect dust events on videos and reconstruct dust trajectories.

The first step is to isolate the dust events appearing on frame. A black and white (BW) video is computed from the raw RGB data using an operation sequence similar to that described in [6]: grayscale conversion, logical filtering (for pixel-size noise reduction), background removal, BW conversion. The latter preprocessing step differs from the usual pixel intensity thresholding used to isolate dust events in previous works [7,8]. A peak detection method is applied to each pixel temporal signal, noted $s(t, x)$, where x is the pixel location on frame and t is the time. A shifted signal $s_{sh}(t, x)$ is created as follows: $s_{sh}(t, x) = s(t + dt, x + dx) + ds$, where dx is of the order of a few pixels, dt a few time indices and ds is a fraction of the peak intensity. Peaks are located where and/or when $s > s_{sh}$. This method shows better results on movies with varying backgrounds since only sudden events are detected, whereas a brutal threshold could keep some long lasting elements the background suppression step could not delete properly, such as hot spots apparition or plasma emission changes. DUMPRO includes other features, such as frame vibration compensation, which were not used for the results presented in this paper.

The second step consists in associating the previously detected dust events together to reconstruct trajectories. The algorithm works using a recurrence method over time: given a dust trajectory reconstructed until the frame t_0 , a probability is associated to every dust detected on the next frame $t_0 + dt$ to be the following point. If the most probable dust on frame $(t_0 + dt)$ has a probability over a given threshold, the point is added to the trajectory, making this method fully automatic. Later on, two successive points on a dust trajectory will be referred to as parent and child, respectively. In DUMPRO, the probability formula that drives the parent/child association depends on two parameters: (i) the distance between potential parent and child: since a dust motion is mostly inertia driven, its velocity vector norm and orientation changes rather slowly with respect to the frame rate of a fast CCD camera (~ 200 Hz in the case of the TV2 camera in KSTAR). Thus the distance between two consecutive points on a trajectory recorded by a CCD camera must not change too drastically. (ii) The difference in apparent size of the potential parent and child: similarly to the previous point, dust temperature and size evolutions are rather slow processes compared to the frame rate of a fast CCD camera. Here is where the algorithm differs from previous works [7,8], which did not take into account the dust apparent size. Let us consider a BW video containing dust events and a dust trajectory reconstructed until frame t_0 . Let i be the final point of the trajectory, on frame t_0 , and j a dust located on frame $t_0 + dt$. The probability for j to be the child of i is written as follows:

$$P(i, j) = \alpha_1 \times \left(\frac{\cos \theta_{i,j} + 1}{2} \right) \times G_{\text{dist}}(d_{i,j}) + \alpha_2 \times G_{\text{size}}(s_{i,j}) \quad (1)$$

where α_i are weights, usually set as $\alpha_1 = 5/6$ and $\alpha_2 = 1/6$, $d_{i,j}$ and $s_{i,j}$ are the distance and apparent size difference between i and j , respectively, G_k are Gaussian functions with parameters to be chosen (center and width), and $\theta_{i,j}$ is the angle between the vectors linking the parent of i to i and i to j . The centers of G_{dist} and G_{size} are the average distance and apparent size difference between two successive points of the dust trajectory up to frame t_0 ,

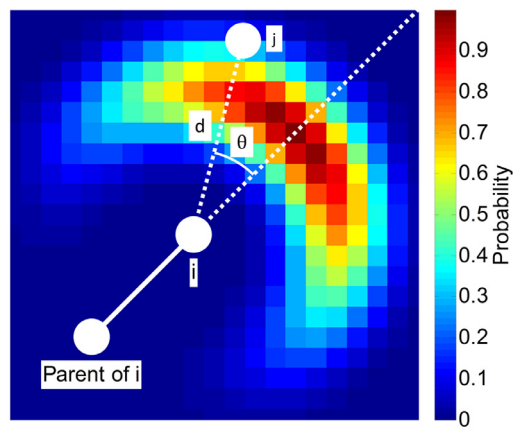


Fig. 1. Map of the probability to find a dust position on frame $t_0 + dt$, given its position at times t_0 (i) and $t_0 - dt$ (Parent of i).

respectively. The widths of G_{dist} and G_{size} are parameters depending on the camera resolution, usually a few pixels. Fig. 1 gives an overview of the probability computation in DUMPRO: an example of trajectory is plotted over probability values for each pixel of the frame.

Results of DUMPRO routines are given in Fig. 3(b) for a movie from the 2015 KSTAR dust injection experiment. Blue circles representing the detected dust events on the whole video are plotted over the superimposed frame and blue lines show the trajectories reconstructed by the algorithm.

3. DUMBO: the dust transport code

In parallel to the image processing routines, a dust transport simulation code has been developed at CEA. Named DUMBO (DUSt Migration in a plasma BOundary), it is based on the Orbital Motion Limited (OML) approach [9]. Like in other dust transport codes, OML expressions are implemented for a spherical dust grain and Maxwellian distributions for plasma particles energy, taking into account a mean flow velocity in the case of ions [10]. The plasma background necessary to compute plasma/dust interactions is an input to DUMBO. It can be obtained either by plasma modeling codes such as SOLEDGE-2D [11] or by experimental measurements [12]. The aim of the present section is to give a quick overview of the model implemented in DUMBO. More details will be presented elsewhere.

3.1. Dust charging

A dust grain immersed in a plasma charges up to the floating potential ϕ_d , which is determined by solving the current balance. Plasma electron and ion currents, noted J_i and J_e , are given by OML [10]. DUMBO also takes into account secondary electron emission (SEE) and thermionic emission (TH) effects.

The SEE yield δ_{see} is computed using the Young–Dekker formula, since it was shown to give more accurate results at scrape-off layer (SOL) relevant energies than the Sternglass one [13], and is integrated over the electron incidence angle and a Maxwellian distribution. Thus δ_{see} depends mainly on the incoming electrons energy (i.e. the electron temperature T_e), the dust material and ϕ_d . Similar expressions to that of MIGRAINE are implemented in DUMBO for $\phi_d \leq 0$ [2]. In the case $\phi_d \geq 0$, secondary electrons are assumed to be reabsorbed by the attracting grain, resulting in $\delta_{see} = 0$.

TH designates the electron emission generated by the temperature increase of a material. The thermionic current J_{th} depends

on the dust material, temperature and ϕ_d and is given by the Richardson–Dushman formula [14].

The current balance can then be solved to find ϕ_d :

$$(1 - \delta_{see})J_e - J_{th} = J_i \quad (2)$$

The dust electric charge Q_d is calculated using the expression $Q_d = 4\pi\epsilon_0 r_d \phi_d$, where ϵ_0 is the permittivity of vacuum and r_d the dust radius [15].

3.2. Equation of motion

Amongst the many forces acting on a dust grain immersed in a plasma, three are kept in the DUMBO model: the Lorentz force, the gravity and the ion drag force F_{id} , whose expression comes from the OML theory [2]. The equation of motion is written:

$$M_d \frac{d\mathbf{V}_d}{dt} = \mathbf{F}_{id} + Q_d(\mathbf{E} + \mathbf{V}_d \times \mathbf{B}) + M_d \mathbf{g} \quad (3)$$

where M_d is the dust mass, \mathbf{V}_d its velocity, \mathbf{E} and \mathbf{B} are the local electric and magnetic fields, respectively, and \mathbf{g} is the acceleration of gravity. The ion drag force is usually the main force acting on dust grains. Nevertheless, the dust radius r_d plays an important role in the amplitude of these forces: given that $\mathbf{F}_{id} \sim r_d^2$, $Q_d \sim r_d$ and $M_d \sim r_d^3$ (neglecting the dependence of ϕ_d on r_d), it appears that gravity plays an important role for large grains.

3.3. Dust heating

The heating equation is written as follows:

$$M_d c_p \frac{dT_d}{dt} = Q_i + Q_e - Q_{see} - Q_{th} - Q_{rad} + Q_{rec} \quad (4)$$

where T_d is the dust temperature, c_p is the T_d dependent heat capacity and Q_k are the different heat fluxes impacting the grain [15]. Q_i and Q_e are the plasma ions and electrons heat fluxes, respectively. Their expressions come from the OML theory, the latter being generally the main source of dust heating. Q_{see} and Q_{th} are the secondary and thermionic electron heat fluxes, given by the Young–Dekker and Richardson–Dushman formulas, respectively. Q_{rad} designs the black body radiation and Q_{rec} is the recombination heat flux. Collected ions are assumed to recombine on the dust surface and form dihydrogen molecules before being released into the plasma. Heat fluxes due to other species are not taken into account, since they have lower densities and carry less energy. Vaporization cooling is neglected and replaced by a T_d saturation on phase transitions, whilst the incoming heating power is directed to this phase change.

3.4. Mass loss

Whilst interacting with the plasma, a dust grain loses mass due to physical sputtering, vaporization/sublimation and, in some cases, chemical sputtering. In DUMBO, the mass loss equation is written:

$$\frac{dM_d}{dt} = \left. \frac{dM_d}{dt} \right|_{\text{sput}} + \left. \frac{dM_d}{dt} \right|_{\text{vap}} \quad (5)$$

where $\left. \frac{dM_d}{dt} \right|_{\text{sput}}$ is the mass loss due to sputtering. The expressions from Behrisch and Eckstein, considering different impacting ions with different energies on different target materials, are implemented in DUMBO [16]. The variation of the sputtering yield with the angle of incidence and the energy distribution function of the incoming particles is taken into account, similarly to what is done in MIGRAINE [2]. $\left. \frac{dM_d}{dt} \right|_{\text{vap}}$ is the vaporization/sublimation mass loss, expressed with the Hertz–Knudsen formula [17].

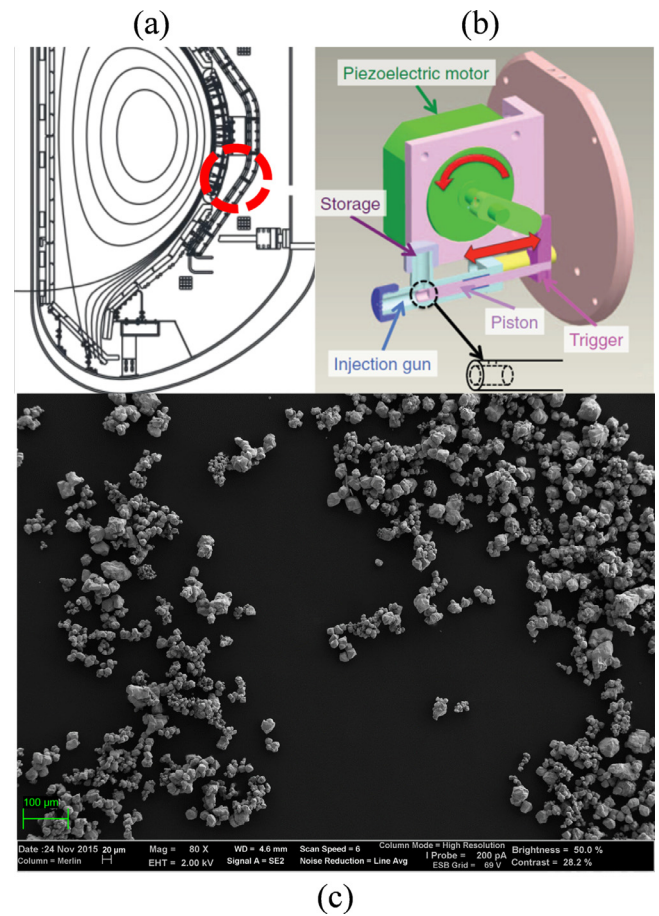


Fig. 2. KSTAR dust injection setup: (a) Injection point location in a poloidal section; (b) Gun-type injector design [5]; (c) MEB image of the injected W powder.

4. Application to the 2015 KSTAR dust injection experiment

Comparing intrinsic and simulated dust trajectories is delicate since CCD cameras do not give access to important dust parameters on which the trajectory depends strongly, such as r_d , T_d , the dust material and distance to the camera. A way to constrain some parameters is controlled dust injection. Such experiments have been performed on various tokamaks (DIII-D, TEXTOR, NSTX, MAST, among others) during the last decade. Details are presented in [18] and the references therein. This section will focus on the dust injection experiment performed in KSTAR during the 2015 campaign, the application of the DUMPRO routines on the video recorded by a fast visible camera and the comparison between measured dust trajectories and some simulated ones generated with DUMBO.

4.1. Dust injection experiment in KSTAR

During the 2015 campaign in KSTAR, dust injection was performed using a gun-type injector, whose design is shown in Fig. 2(b). The chosen powder falls from the storage reservoir into the canon by gravity and is propelled into the plasma by a piston, which is put into motion by a piezo-electric motor. More details on the KSTAR gun-type injector can be found in [5]. The injection point was located slightly below the outer mid plane, as shown in Fig. 2(a), and the injection velocity was a few m/s, directed inwards. The injected amount was ~ 2 mg of W powder per shot. The grains size distribution is wide, ranging from $\sim 10 \mu\text{m}$ up to $\sim 100 \mu\text{m}$. A MEB image in Fig. 2(c) shows that dust grains are

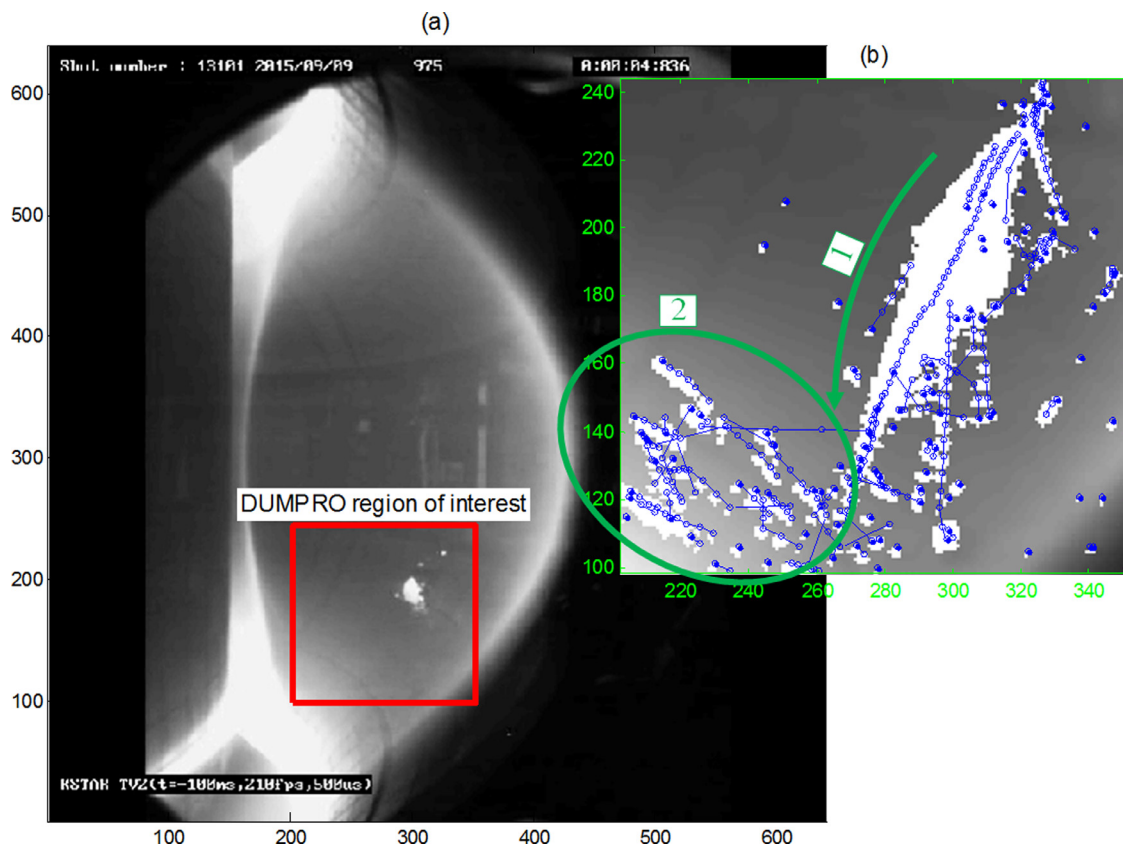


Fig. 3. Application of the DUMPRO routines on the KSTAR #13101 TV2 video: (a) Frame at $t = 4.836$ s with the DUMPRO region of interest in red; (b) Dust trajectories (blue) reconstructed on the whole video over the superimposed frame, zoomed in the region of interest, with the two dust behaviors, *case 1* and *case 2*, underlined in green. (For interpretation of the references to colour in this figure legend, the reader is referred to the web version of this article.)

mostly accreted into clusters of $\sim 100\ \mu\text{m}$ size and irregular shape. Injected dust trajectories were recorded by the fast CCD visible camera installed in KSTAR. Fig. 3(a) shows a snapshot of the video. The several milligrams of W powder injected heat up upon entering the SOL and start emitting light in the visible spectrum, generating the bright region located in the red square in Fig. 3(a).

4.2. Image processing using DUMPRO

The DUMPRO routines were applied to the video in order to get the dust trajectories. Results found by the algorithm can be seen in Fig. 3(b). Detected dust trajectories are plotted in blue over the superimposed frame of the whole video. From the image processing results, two distinct dust behaviors were observed. First, a large white cloud falls from the dust injection point towards the divertor region. Labeled as *case 1*, this main trajectory corresponds to the powder that just left the injector and falls downwards due to gravity. This behavior is consistent with the DUMBO model since the injected W powder is accreted into $\sim 100\ \mu\text{m}$ clusters, a size for which gravity is the dominant force. Little to no toroidal motion is seen on the video. At the end of the *case 1* trajectory, dust gets closer to the wall and cools down enough to stop emitting light in the visible spectrum, and they disappear from the video. During the end of the *case 1* trajectory, other dust grains are observed on the bottom-left corner of Fig. 3(b), being more isolated and having a toroidal motion. These dust trajectories will be labeled as *case 2*. Assuming that they have a radius of $\sim 10\ \mu\text{m}$, the dominant force acting on them will be the ion drag, which is roughly oriented along the magnetic field lines.

The dust grains from *case 2* can either be the result of grains from *case 1* having experienced a bouncing dust/wall collision, or

grains that were isolated from the dust cluster of *case 1* at some point during its falling towards the divertor. In both cases it is not illegitimate to consider that the trajectories in *case 2* are isolated $\sim 10\ \mu\text{m}$ dust grains since the $\sim 100\ \mu\text{m}$ size clusters from *case 1* could be broken upon the eventual dust/wall collision or simply due to internal forces. Since the end of the *case 1* trajectory cannot be observed with the CCD camera due to too low dust temperature, no conclusions can be made on this point and *cases 1* and *2* will be treated separately later on.

4.3. Comparison with DUMBO simulations and discussion

Comparison of observed dust trajectories with simulations has already been performed on MAST [19], LHD [20] and TEXTOR [21], using stereoscopic observations in the latter case. Since no binocular view is available in KSTAR, the dust trajectories given by DUMPRO are 2D, result of 3D trajectories projected in the camera sensor plane. In order to compare with simulated dust trajectories generated with DUMBO, 3D trajectories are recreated from the measured 2D ones by assuming the following: (i) For *Case 1*, since the dust are heavy ($r_d \sim 100\ \mu\text{m}$) and have a gravity driven motion, we assume the trajectory to remain at a chosen toroidal angle. (ii) Concerning *Case 2*, dust grains are lighter ($r_d \sim 10\ \mu\text{m}$) and have an ion drag force driven motion, which is roughly oriented along the magnetic field lines. Thus we assume the dust to remain in a chosen flux tube. The toroidal angle where the *case 1* trajectory was placed was chosen in a way that it remains mostly in the SOL without crossing the wall surface. The *case 2* trajectories were placed on flux tubes as far as possible from the plasma core while ensuring the existence of a solution.

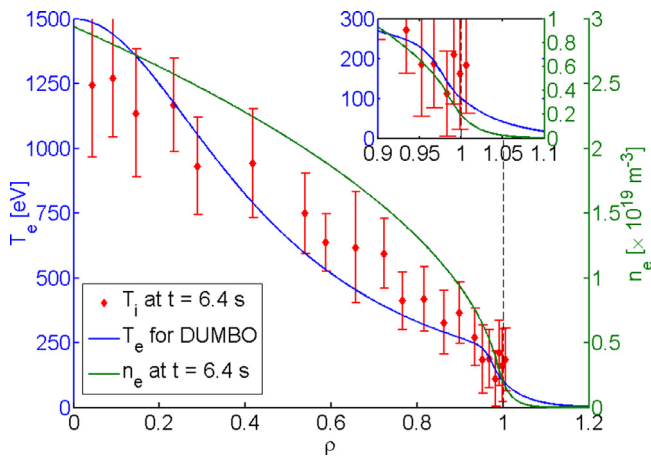


Fig. 4. T_i (red) and n_e (green) profiles at $t = 6.4$ s from charge exchange spectroscopy and line integrated density, respectively. T_e profile (blue) obtained by fitting the T_i one. (For interpretation of the references to colour in this figure legend, the reader is referred to the web version of this article.)

Note that in order to make this 2D-to-3D extrapolation some features of the CCD camera must be known: position in the vessel, focal length, sensor size, among others. A simple pinhole camera model was used, and the camera parameters were chosen to match the background (wall) frame as accurately as possible. Results of the 2D-to-3D extrapolation process are shown for the *case 1* trajectory and three trajectories from *case 2* in Fig. 5.

For each of the four trajectories extrapolated in 3D from the DUMPRO routines results, simulations were made using the DUMBO code. The plasma background was determined using several diagnostics on discharge #13101: EFIT data for the magnetic equilibrium and poloidal magnetic field, charge exchange spectroscopy for the ion temperature (T_i) profile, line integrated density for the electron density (n_e). Profiles were extended in the SOL using exponential decays respecting a C^1 match with the core profiles. The n_e profile was determined from the integrated density using a square root profile in the core, and we assumed $T_e = T_i$.

Finally, quantities were assumed to remain constant over flux surfaces. Profiles for n_e and T_i are provided in Fig. 4. The toroidal magnetic field was ~ 3 T, and the plasma ions flow velocity map can be seen in the background of Fig. 5(a). The ion flow is predominantly parallel, even though $\mathbf{E} \times \mathbf{B}$ and $\nabla \mathbf{B} \times \mathbf{B}$ drift velocities are taken into account.

In the simulations, the dust grains were initiated at the same location and with the same velocity vector as the first point of each experimental trajectory. The initial dust radii were $100 \mu\text{m}$ for *case 1* and $10 \mu\text{m}$ for *case 2*. Results are plotted in Fig. 5 along with the experimental trajectories extrapolated in 3D. One can see that the agreement between experimental and simulated trajectories is satisfying in *case 1*, since they are both dominated by gravity. Discrepancy can be seen on the toroidal trajectory, since the ion drag force, which is dominated by gravity yet not negligible, pushes the simulated dust in the toroidal direction, counter-clockwise. Concerning *case 2*, if simulated trajectories seem close at first, they end up to be much shorter than the experimental ones. This discrepancy can be explained by several effects.

First, some cooling mechanisms are not yet accounted for in DUMBO, since SEE is neglected for positively charged dust grains and vaporization/sublimation latent heat cooling is replaced with a boiling/sublimation point. The implementation of these phenomena is under progress.

Second, it is known that the OML approach used in DUMBO (and other dust simulation codes) presents severe limitations, since it assumes the absence of barriers in the effective potential energy. Effective potential barriers can trap a non negligible part of the slow incoming ions if r_d gets to the order of the screening length, which is $\sim 10 \mu\text{m}$ in our case [22]. On the other hand, if the emitted electron flux gets close to the incoming one, potential wells can form and reduce the electron emission itself [1]. Another OML limitation appears whilst plasma electrons become magnetized with respect to r_d : their gyration motion induces a reduction in the incoming electron flux [23]. These three effects are not accounted for in DUMBO and impact the dust charging and heating.

Third, in the present version of the code, the material ablated or vaporized from the grain does not affect it nor the surrounding plasma. To be accurate, the ablated material can form a cloud

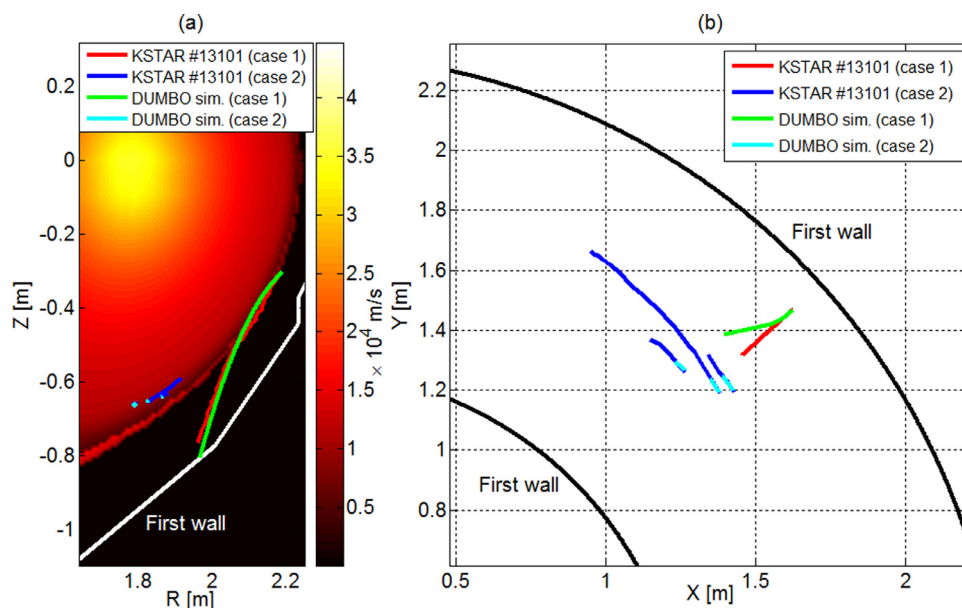


Fig. 5. KSTAR dust injection experiment – comparison between dust experimental trajectories, reconstructed with DUMPRO, and simulated ones made with DUMBO: (a) in a poloidal cross-section, above the ion flow velocity map, with the first wall geometry in white; (b) view from the top of the machine, with the first wall geometry at the mid plane in black.

shielding the grain from plasma heat fluxes. In Ref [24], the dust radius above which vapor shielding effects become non negligible was shown to be $\sim 1 \mu\text{m}$ (for W and under the plasma parameters relevant in this study), which is below the dust sizes used in our simulations. Vapor shielding models have shown a reduction of the evaporation rate up to an order of magnitude [25].

Still, this overheating tendency has been reported on other codes based on the same model, namely DUSTT, DTOKS and MIGRAINE. The MIGRAINE code was used to compare with dust injected in TEXTOR. The dust grains were smaller than in our study ($< 5 \mu\text{m}$) and injected from the top of the machine. A similar overheating trend was observed [21]. Compensation for overheating was accomplished in the DUSTT code by including a large empirical reduction coefficient to the incoming heat flux [26]. Concerning DTOKS, larger dust sizes were used in the simulations to reproduce accurately the experimental dust lifetimes [19].

5. Conclusions

Image processing routines (DUMPRO) have been developed and allow detection of dust trajectories on a CCD camera video. A dust transport simulation code (DUMBO) for trajectories modeling is also available. 2D-to-3D extrapolation of measured dust trajectories was applied in the KSTAR dust injection experiment example, confirming that lighter W dust grains are more sensitive to the ion drag force than larger ones. Comparison between measurements and simulations showed discrepancies due to OML limitations and/or to the lack of a vapor shielding model. Improvements on these aspects are compulsory if DUMBO is to be used to predict the behavior of injected dust in the WEST tokamak.

Acknowledgment

This research was partially supported by Ministry of Science, ICT, and Future Planning under KSTAR project and was partly supported by National Research Council of Science and Technology (NST) under the international collaboration & research in Asian countries (PG-1314).

References

- [1] S.I. Krasheninnikov, R.D. Smirnov, D.L. Rudakov, *Plasma Phys. Controlled Fusion* 53 (8) (2011) 083001.
- [2] L. Vignitchouk, P. Tolias, S. Ratynskaia, *Plasma Phys. Controlled Fusion* 56 (9) (2014) 095005.

- [3] A.Y. Pigarov, S.I. Krasheninnikov, T.K. Soboleva, T.D. Rognlien, *Phys. Plasmas* 12 (2005) 122508. <http://dx.doi.org/10.1063/1.2145157>.
- [4] M. Bacharis, M. Coppins, J.E. Allen, *Phys. Plasmas* 17 (2010) 042505. <http://dx.doi.org/10.1063/1.3383050>.
- [5] H.Y. Lee, S.-H. Hong, J. Hong, S.H. Lee, S. Jang, J. Jang, T. Jeon, J.S. Park, W. Choe, *Rev. Sci. Instrum.* 85 (2014) 11D862. <http://dx.doi.org/10.1063/1.4886958>.
- [6] S.-H. Hong, C. Grisolia, P. Monier-Gabet, T.S. Team, *J. Nucl. Mater.* 390–391 (2009) 100–102. <http://dx.doi.org/10.1016/j.jnucmat.2009.01.120>.
- [7] N. Endstrasser, F. Brochard, V. Rohde, M. Balden, T. Lunt, S. Bardin, J.-L. Briannon, R. Neu, *J. Nucl. Mater.* 415 (1) (2011) S1085–S1088. <http://dx.doi.org/10.1016/j.jnucmat.2010.07.045>, Proceedings of the 19th International Conference on Plasma-Surface Interactions in Controlled Fusion.
- [8] W.U. Boegli, A.L. Roquemore, R. Maqueda, *Rev. Sci. Instrum.* 79 (10) (2008). <http://dx.doi.org/10.1063/1.2965001>.
- [9] H.M. Mott-Smith, I. Langmuir, *Phys. Rev.* 28 (1926) 727–763, doi:10.1103/PhysRev.28.727.
- [10] C.T.N. Willis, M. Coppins, M. Bacharis, J.E. Allen, *Phys. Rev. E* 85 (2012) 036403, doi:10.1103/PhysRevE.85.036403.
- [11] H. Bufferand, G. Ciraolo, L. Isoardi, G. Chiavassa, F. Schwander, E. Serre, N. Fedorczak, Ph. Ghendrih, P. Tamaun, *J. Nucl. Mater.* 415 (2011) S589–S592. <http://dx.doi.org/10.1016/j.jnucmat.2010.11.037>.
- [12] J.P. Gunn, R. Dejarnac, P. Devynck, N. Fedorczak, V. Fuchs, C. Gil, A. Kocan, M. Komm, M. Kubic, T. Lunt, A. Monier-Garbet, J.Y. Pascal, F. Saint-Laurent, *J. Nucl. Mater.* 438 (2013) S184–S188. <http://dx.doi.org/10.1016/j.jnucmat.2013.01.055>.
- [13] P. Tolias, *Plasma Phys. Controlled Fusion* 56 (12) (2014) 123002.
- [14] S. Dushman, *Rev. Mod. Phys.* 2 (1930) 381–476, doi:10.1103/RevModPhys.2.381.
- [15] G.L. Delzanno, X. Tang, *Phys. Plasmas* 21 (2014) 022502. <http://dx.doi.org/10.1063/1.4864190>.
- [16] R. Behrisch, W. Eckstein, *Sputtering Part. Bombardment*, 110, Springer Berlin Heidelberg, 2007, doi:10.1007/978-3-540-44502-9.
- [17] R. Marek, J. Straub, *Int. J. Heat Mass Transfer* 44 (2001) 39–53. [http://dx.doi.org/10.1016/S0017-9310\(00\)00086-7](http://dx.doi.org/10.1016/S0017-9310(00)00086-7).
- [18] S. Ratynskaia, C. Castaldo, H. Bergsaker, D. Rudakov, *Plasma Phys. Controlled Fusion* 53 (7) (2011) 074009.
- [19] G.D. Temmerman, M. Bacharis, J. Dowling, S. Lisgo, *Nucl. Fusion* 50 (10) (2010) 105012.
- [20] M. Shoji, H. Kasahara, M. Tokitani, T. Seki, K. Saito, S. Kamio, R. Seki, Y. Tanaka, A. Pigarov, R. Smirnov, G. Kawamura, H. Tanaka, S. Masuzaki, Y. Uesugi, T. Mutoh, T.L.E. Group, *Nucl. Fusion* 55 (5) (2015) 053014.
- [21] A. Shalpegin, L. Vignitchouk, I. Erofeev, F. Brochard, A. Litnovsky, S. Bozhenkov, I. Bykov, N. den Harder, G. Sergienko, *Plasma Phys. Controlled Fusion* 57 (12) (2015) 125017.
- [22] V. Fortov, A. Ivlev, S. Khrapak, A. Khrapak, G. Morfill, *Phys. Rep.* 421 (1–2) (2005) 1–103. <http://dx.doi.org/10.1016/j.physrep.2005.08.007>.
- [23] V.I. Demidov, S.V. Ratynskaia, K. Rypdal, *Rev. Sci. Instrum.* 73 (10) (2002) 3409–3439. <http://dx.doi.org/10.1063/1.1505099>.
- [24] B.T. Brown, R.D. Smirnov, S.I. Krasheninnikov, *Phys. Plasmas* 21 (2) (2014). <http://dx.doi.org/10.1063/1.4866599>.
- [25] S.I. Krasheninnikov, E.D. Marenkov, *J. Nucl. Mater.* 463 (2015) 869–872. <http://dx.doi.org/10.1016/j.jnucmat.2014.10.077>.
- [26] R.D. Smirnov, S.I. Krasheninnikov, A.Y. Pigarov, A.L. Roquemore, D.K. Mansfield, J. Nichols, *J. Nucl. Mater.* 415 (1) (2011) S1067–S1072. <http://dx.doi.org/10.1016/j.jnucmat.2011.01.004>, Proceedings of the 19th International Conference on Plasma-Surface Interactions in Controlled Fusion.